THE JOURNAL OF PHYSICAL CHEMISTRY B

Article

pubs.acs.org/JPCB

Calculating the Hydrodynamic Volume of Poly(ethylene oxylated) Single-Walled Carbon Nanotubes and Hydrophilic Carbon Clusters

Alfredo D. Bobadilla,[†,‡] Errol. L. G. Samuel,[¶] James M. Tour,*[,¶,∥,⊥] and Jorge M. Seminario*[,†,‡,§]

[†]Department of Chemical Engineering, [‡]Department of Electrical and Computer Engineering, and [§]Materials Science and Engineering Graduate Program, Texas A&M University, College Station, Texas 77843, United States, and [¶]Department of Chemistry, [∥]Department of Mechanical Engineering and Materials Science, and [⊥]Smalley Institute for Nanoscale Science and Technology, Rice University, 6100 Main Street, Houston Texas 77005, United States

ABSTRACT: Poly(ethylene glycol) (PEG) functionalization of carbon nanotubes (CNTs) is widely used to render CNTs suitable as vectors for targeted drug delivery. One recently described PEGylated version uses an oxidized single-walled carbon nanotube called a hydrophilic carbon cluster (HCC). The resulting geometric dimension of the hybrid PEG−CNT or PEG−HCC is an important factor determining its ability to permeate the cellular membrane and to maintain its blood circulation. Molecular dynamics (MD) simulations were performed to estimate the maximum length and width dimensions for a PEGylated single-walled carbon nanotube in water solution as a model for the PEG−HCC. We ensured maximum PEGylation by functionalizing each carbon atom in a CNT ring with an elongated PEG molecule, avoiding overlapping between PEGs attached to different CNT rings. We suggest that maximum PEGylation is important to achieve an optimal drug delivery platform.

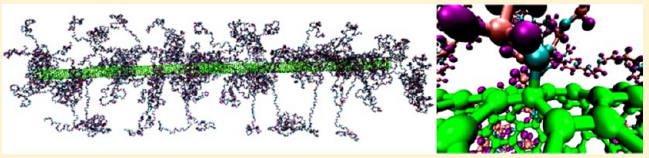

INTRODUCTION

Carbon nanotubes constitute an emerging class of drug delivery platforms.[1,2] The very small dimension of carbon nanotubes, especially in the radial direction, ensures efficient circulation through blood.[3] A very effective version of this consists of shortened (40−60 nm long) oxidized carbon nanotubes[4,5] to which solubilizing addends,[6] namely 5000 molecular weight poly(ethylene glycol) moieties, have been attached.[7] The entire constructs are termed poly(ethylene glycol)-functionalized hydrophilic carbon clusters (PEG−HCCs) and these have recently been shown to have enormous efficacy and ultralow toxicity.[8,9] These PEG−HCCs are very short compared to the CNTs used in earlier studies—they are short enough that they show efficient clearance via the kidneys and nontoxicity in mammals—and are proving to be exceedingly effective for in vitro and in vivo drug delivery.[10−12]

A considerable number of drugs with high therapeutic efficacy are of hydrophobic nature.[13,14] We would expect some affinity of these drugs to CNTs, as CNTs themselves are inherently hydrophobic.[15] In addition, in order to maintain the properties of these drugs, it is preferable that they be noncovalently loaded onto the CNT construct.[7,16] Studies of hydrophobicity in toxicity prediction were performed by Cronin[17] and Moyano et al.;[18] however, further research is needed to explore biological responses to carbon nanomaterials. Fortunately, PEG has excellent solubility in water, and CNT functionalization with PEG imparts increased solubility in water solutions as well as reduced toxicity.[19] We therefore expect PEG−CNT constructs to have strategically localized hydrophobic and hydrophilic sites, making them excellent therapeutic carriers. HCCs do in fact have hydrophobic domains which ensure drug sequestration, but they also have oxidized sites for covalent PEG attachment. PEG−HCCs have demonstrated very high effectiveness for both untargeted and antibody-targeted delivery, but little is known regarding their actual hydrodynamic volume when water-association is manifested. This question is addressed here using a shortened single-walled carbon nanotube as the central core and PEG addends.

Molecular simulations provide complementary information to experimental techniques by enabling the analysis of the structure and fast dynamics with atomistic detail.[20−22] Classical molecular dynamics simulations are playing an increasingly important role in drug discovery[23,24] to the point that they are becoming essential and not just complementary. Simulation techniques are used for example in the identification of binding sites[25] and prediction of ligand binding energies[26,27] and to understand the atomistic energetics and mechanics of binding.[28] CHARMM is a widely used force field for molecular dynamics simulations and it has been parametrized for different types of biological molecules,[29−31] for ethers (CHARMM35),[32] for hybrid nanomaterials[33−35] and recently also for drug-like molecules.[36] A revised version CHARMM-35r for ethers reported by Lee et al.,[37] refitted the OCCO dihedral potential energy, yielding excellent agreement with experiment for persistence lengths and hydrodynamic radii at high and low molecular weights.

In the present work, we perform molecular dynamics calculations on a PEG 114-mer in water to obtain a PEG with globular shape. This 114-mer affords a 5040 molecular weight chain, the typical chain length found in PEG−CNTs for biological applications.[7,16] We then analyze the maximum number of PEG molecules that can possibly be covalently linked to a CNT sidewall. Finally, after equilibration at room temperature, we analyze the geometry of the PEG−CNT construct.

Received: May 31, 2012
Revised: December 2, 2012

   dx.doi.org/10.1021/jp305302y | J. Phys. Chem. B XXXX, XXX, XXX−XXX

METHODOLOGY

So far, to our knowledge, the precise structure of a HCC complex has not been reported yet and we consider a single-walled CNT (SWCNT) as the simplest structural model to represent a hydrophobic carbon nanostructure since HCC is derived from oxidation of SWCNT by a mixed acid.[7]

We employ the CHARMM force field (eqs 1−3 and Tables 1−5)[29] as implemented in the LAMMPS software.[38]

Table 1. Stretching Parameters for Water,[43] Carbon Nanotube (CNT),[29,40] and Poly(ethylene glycol) (PEG).[32]

molecule	bond	k_b (kcal/mol/Å^2)	b_0 (Å^2)
water	OH	450	0.9572
PEG	CC	222.5	1.53
	CO	360	1.415
	CH	309	1.111
CNT	CC	600	1.335
CNT-PEG link	CO	480	1.375

Table 2. Bending Parameters for Water,[43] CNT,[29,40] and PEG[32]

molecule	angle	k_θ (kcal/mol)	θ_0 (deg)	K_{UB} (kcal/mol/Å^2)	r_{UB} (Å^2)
water	HOH	55	104.52	0	0
PEG	OCC	45	111.5	0	0
	COC	95	109.7	0	0
	HCH	35.5	109	5.4	1.802
	CCH	26.5	110.1	22.53	2.179
	OCH	60	109.5	0	0
CNT	CCC	40	120	35	2.4162
CNT-PEG link	CCO	45	104.5	0	0
	CCC	45	104.5	35	2.4162

Table 3. Torsion Parameters for CNT[29,40] and PEG[32]

molecule	dihedral	k_ϕ (kcal/mol)	n	δ (deg)	type of bonding[a]
PEG	OCCO	0.25	1	180	O−C−C−O
	OCCO	1.24	2	0	O−C−C−O
	COCC	0.43	3	0	C−O−C−C
	HCCO	0.19	3	0	H−C−C−O
	HCOC	0.284	3	0	H−C−O−C
	HCCH	0.19	3	0	H−C−C−H
CNT	CCCC	3.1	2	180	C≃C≃C≃C
CNT-PEG link	COCC	0.33	3	0	C−O−C−C

[a]Bonding notation: A−B is single covalent bond and A≃B is resonant covalent bond.

Table 4. Torsion Parameters for the OCCO Dihedral Angles Corresponding to the OCE-CCT2-CCT2-OCE (Atom Types)[a]

		k_ϕ (kcal/mol)	
n	δ (deg)	C35[32]	C35r[37]
1	180	0.25	0.59
2	0	1.24	1.16

[a]CCT2 is the C(sp3)H2 carbon; OCE is ether oxygen in linear ether(s); HCT2 is alkane H attached to C(sp3)H2.

Covalent bonded interactions parameters and charges for PEG were taken from CHARMM35 version for ethers[32] and the Lennard-Jones parameters were taken from the work reported by Kenzabu Tasaki.[39] Bonds, angles, and dihedrals were identified in a PEG molecule (Figure 1) to assign the corresponding force field parameters. The CNT was modeled with CHARMM

Table 5. Lennard-Jones Parameters for Water,[43] PEG,[39] and CNT[29,40]

molecule	pair interaction	ϵ_{ij} (kcal/mol)	$R_{0_{ij}}$ (Å)
PEG	CC	0.095	3.44
	OO	0.199	2.85
	HH	0.098	3.0
	CO	0.138	3.15
	CH	0.031	3.23
	OH	0.044	2.93
water	O	0.1521	3.1507
	H	0.046	0.4
	OH	0.0836	1.7753
CNT	CC	0.11	3.563595

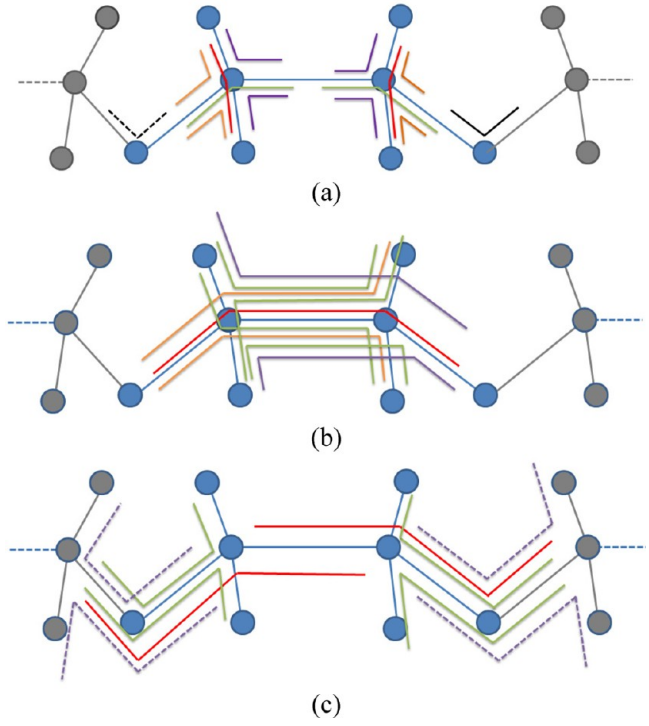

Figure 1. Angles and dihedrals identified in a repeat unit (mer) C_2H_4O of PEG molecule. (a) Angles are identified as OCC (green), COC (black), HCH (red), CCH (purple), and OCH (orange). (b) Dihedrals in every mer are identified as OCCO (red), OCCH (orange), HCCO (purple), and HCCH (green). (c) Dihedrals at the interface between mers are identified as CCOC (red) and HCOC (green).

parameters[40−42] for a benzene molecule, and the water solvent with the TIP3P model of Jorgensen.[43]

$$V = \sum_b k_b(b - b_0)^2 + \sum_\theta k_\theta(\theta - \theta_0)^2 + \sum_{UB} K_{UB}(r - r_{UB})^2 + \sum_\phi k_\phi[1 + \cos(n\phi - \delta)] + \sum_{nb} \epsilon_{ij}\left[\left(\frac{R_{0_{ij}}}{r_{ij}}\right)^{12} - \left(\frac{R_{0_{ij}}}{r_{ij}}\right)^{6}\right] + \frac{q_i q_j}{\varepsilon r_{ij}} \quad (1)$$

The first sum in eq 1 corresponds to the harmonic stretching terms (Table 1), where k_b are the force constants and b_0 are the equilibrium bond lengths of all bonds; thus, this sum yields the total bond stretching energy, which depends directly on the

dx.doi.org/10.1021/jp305302y | J. Phys. Chem. B XXXX, XXX, XXX−XXX

Table 6. Atomic Charges Defined as Multiple of Electron Charge for Water,[43] PEG,[39] and CNT[29,40]

molecule	atom	q_i
PEG	C	−0.01
	O	−0.34
	H	0.09
water	O	−0.83
	H	0.415
CNT	C	0.0

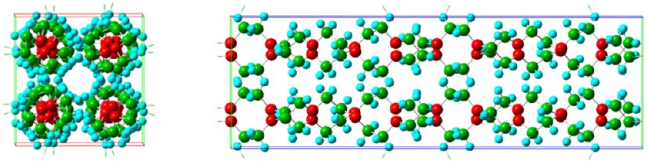

Figure 2. (a) Cross-sectional and (b) lateral view of a unit cell for PEG structure taken from The Cambridge Crystallographic Data Centre. Atoms are color coded: carbon (green), oxygen (red), and hydrogen (cyan).

instantaneous bond lengths, b, of all bonds. The second sum corresponds to bending terms (Table 2), where k_θ are the angle force constants, θ_0 are the equilibrium angles and θ are all the instantaneous angle values. The third sum, the Urey–Bradley component, accounts for angle bending due to 1,3 nonbonded interactions in the three-bonded atoms forming the angle, where k_{UB} is the respective force constant, r_{UB} are equilibrium distances between the 1,3 atoms, and r the instantaneous distances between the 1,3 atoms. The fourth sum corresponds to torsion parameters (Table 3), where k_ϕ are the dihedral force constants, n are the multiplicities of the function, δ are the phase shifts and ϕ the instantaneous dihedral angles. The last sum corresponds to nonbonded parameters where ϵ_{ij} are the depth of the Lennard-Jones potential well, $R_{0_{ij}}$ are the distance at which the corresponding potential is zero (Table 4), ε is the effective dielectric constant, q_i and q_j are atomic charges, and r_{ij} is the instantaneous distance between atoms i and j (Table 5).

Our intention is to gain a qualitative physical picture of the PEG–CNT construct in water without going through an extensive force field parametrization for the PEG–CNT link. Several of these geometries follow earlier ab initio[44−48] and MD[49−51] calculations. The C–O bond coefficients at the PEG–CNT link were considered to be an average value of C═C bond coefficients in the CNT and C–O bond coefficients in the PEG molecule. The dihedral energy coefficient C–O–C–C at the PEG–CNT link was considered to be 0.33 kcal/mol smaller than the one in a PEG molecule (0.43 kcal/mol) to speed

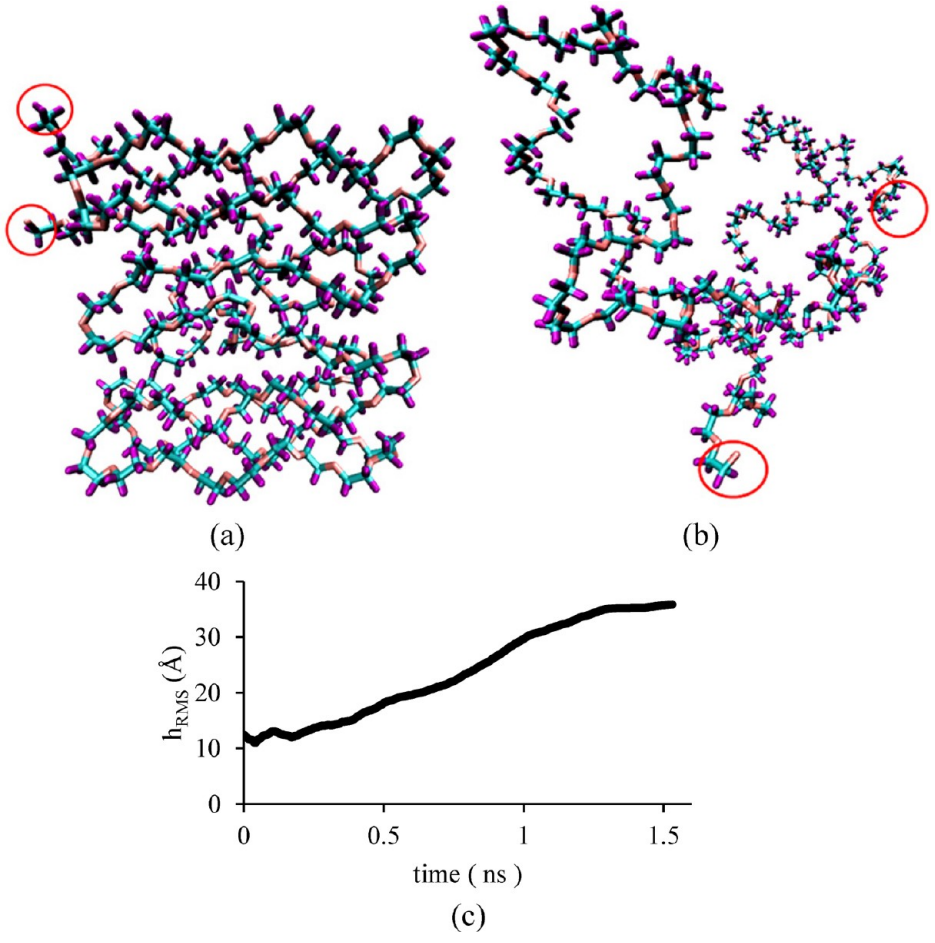

Figure 3. (a) PEG initial structure, before energy minimization and (b) PEG final structure at 300 K for MD simulation. Water molecules are omitted for visualization purposes. Atoms are color coded: oxygen (cyan), carbon (orange), and hydrogen (purple). Red circles highlight the PEG ends. (c) Time evolution of root-mean squared end-to-end distance for the PEG molecule.

dx.doi.org/10.1021/jp305302y | J. Phys. Chem. B XXXX, XXX, XXX–XXX

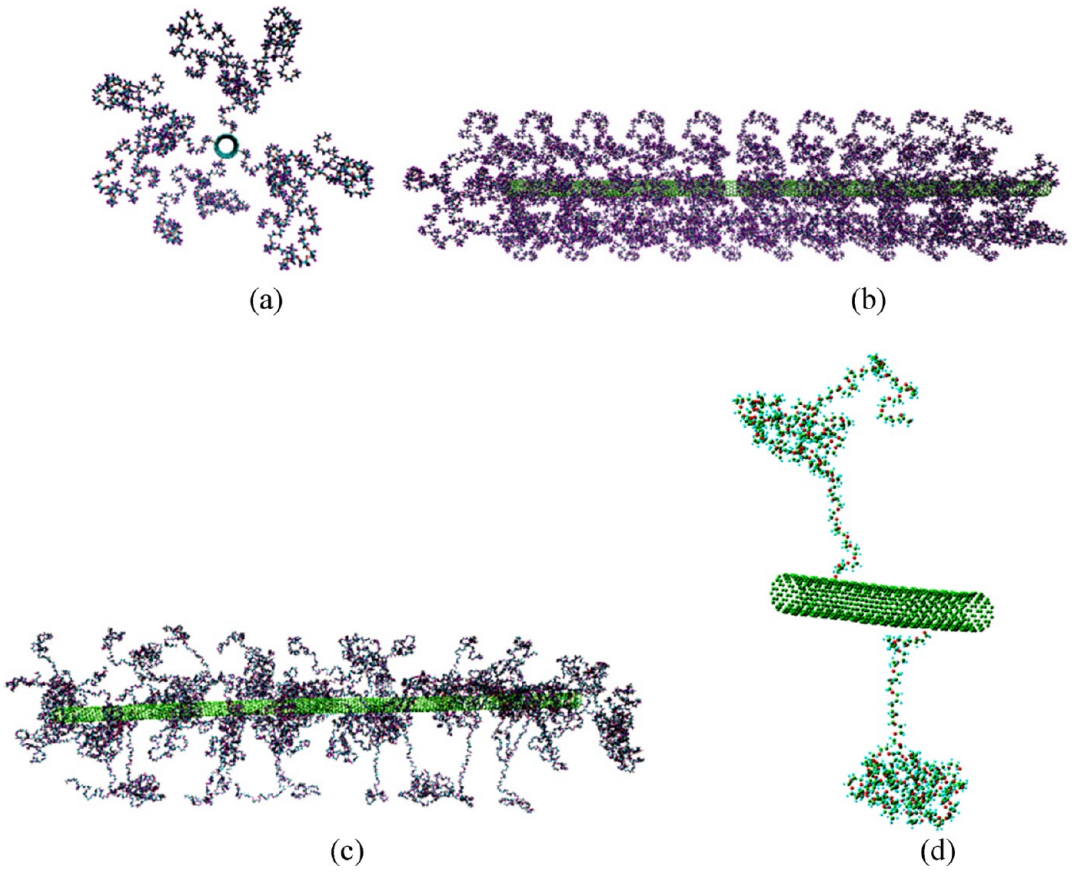

Figure 4. (a) Side view of initial structure. (b) PEG−CNT initial structure, including 40 PEG molecules, before energy minimization. (c) PEG−CNT final structure at 300 K for MD simulation. Water molecules are omitted for visualization purposes. (d) PEG molecules attached to the CNT sidewall show globular and linear segments. Structure was extracted from PEG−CNT final conformation at 300 K.

up conformational changes and allow short time analysis of geometry.

Simulations are performed with the original C35 model;[32] however, a revised version C35r has been reported by Lee et al.[37] After careful check of the revised parameters, we found that the only difference pertaining to our calculations is for the dihedral OCCO angles as shown in Table 4.

The net effect of the correction is practically irrelevant to our calculations. The torsional barrier with the C35 version for this dihedral angle is 2.73 kcal/mol and the corrected value is 2.95 kcal/mol with maxima and minima laying exactly at the same points in both versions. Since one practical technique performing minimizations in MM is to reduce the value of the torsional barriers and then increase them to their correct values, we continue the simulations with the corrected values.

The Lorentz−Berthelot mixing rule is applied to determine Lennard-Jones parameters for interactions between atoms of different type according to

$$\varepsilon_{ij} = \sqrt{\varepsilon_i \times \varepsilon_j} \tag{2}$$

and

$$R_{0_{ij}} = \frac{R_{0_i} + R_{0_i}}{2} \tag{3}$$

Prior to every molecular dynamics simulation, an energy minimization is performed to ensure an initial structure close to a local minimum in the potential energy landscape. The minimization algorithm used is the Polak−Ribiere version of the conjugate gradient algorithm.[52]

A fluid can be subject to a constant pressure, constant temperature, or constant temperature and pressure.[53] An isothermal−isobaric (NPT) ensemble is usually employed for MD simulations of polymers in water. This ensemble corresponds most closely to laboratory conditions with a flask open to ambient temperature and pressure. We are mainly interested on PEG−HCC for drug delivery applications in which case the complex will penetrate the cell membrane and therefore a pressure control is not appropriate.

Therefore, all molecular dynamics simulations are performed under a canonical ensemble (NVT) with a 2 fs time step, temperature controlled by a Nose−Hoover thermostat[54,55] with a 200 fs damping parameter, and 30 Å cutoff distance for nonbonded interactions. To compute long-range Coulombic interactions, a particle−particle particle-mesh solver (Hockney)[56] was employed with 10^{-4} accuracy on relative error in forces. The software PACKMOL[57] is used to construct the initial configuration of the system. Visualization of trajectories is performed using the Visual Molecular Dynamics (VMD) software.[56]

Our PEG molecule was built with data from crystallographic studies by French et al.[58] (Figure 2) available at The Cambridge Crystallographic Data Centre Web page. Three unit cells of the crystal structure CCDC 707050 were modified to obtain a PEG 114-mer length.

dx.doi.org/10.1021/jp305302y | J. Phys. Chem. B XXXX, XXX, XXX−XXX

RESULTS AND DISCUSSION

A PEG 114-mer (Figure 3a) was placed at the center of a cubic box of edge length 80 Å with 16 500 water molecules. The temperature was increased from 0.1 to 300 K in a 50 ps linear ramp followed by an equilibration at 300 K for 1.05 ns until the root-mean-squared (RMS) end-to-end distance (h) of PEG was almost constant (Figure 3c). During this equilibration, the PEG molecule tends to adopt a globular shape (Figure 3b).

The initial PEG structure was not random but derived from X-ray crystal structure reported by French et al.[58] and therefore we do expect a 1.5 ns MD run to be enough time for equilibration. Furthermore, we do expect large fluctuations in the root-mean-squared end-to-end distance (h^{rms}); as a reference, a PEO 158-mer shows an oscillation of hrms from ~40 to ~75 Å[59] in a 800 ns MD run. In the present work, the PEG molecule is shorter, 114-mer length, therefore, the 35 Å reached during the short equilibration is a good reference of the minimum value in the full oscillation range of h^{rms}. We are also interested comparing this minimum value to the h^{rms} value in the PEG–HCC model.

From single PEG equilibration in water solvent, the last structural configuration for PEG was taken as a reference to construct a PEGylated CNT. The PEG chain is terminated by oxygen atoms at both ends (Figure 3b).

In the first PEGylation test, four PEG molecules are covalently attached to the CNT sidewall (Figure 4a) every 34 Å. In total, 40 PEG molecules are attached to a 33.94 nm long single-walled (12,0) CNT (Figure 4b). Bond, angle, and dihedral force field parameters for atoms at the PEG–CNT interface are considered the same as those for a PEG molecule. The construct is solvated with 146 997 water molecules in a 380 × 120 × 120 Å^3 simulation box. Molecular dynamics was performed, bringing the system to room temperature in 50 ps following a linear temperature ramp with time, at which point the system was equilibrated for 50 ps at room temperature. We observed a tendency for elongation in PEG molecules (Figure 4c). We took one of the PEG structures showing the largest elongation (Figure 4d) as a reference for a second test on a PEGylated CNT, aiming to achieve maximum PEGylation.

To fully justify the results obtained from MD simulations of PEGylated CNT, we cite experimental results reported by Hong et al.[60] on atomic force microscopy (AFM) measurements of PEGylated single-walled carbon nanotube in which SWCNT diameter was 1 nm and PEG molecular weight was 5 kDa. According to the AFM measurements, the average diameter for the PEG–CNT complex is 15 nm which corresponds to a radial thickness of 70 Å for the polymer wrapping CNT.[60]

Our carbon nanotube (0.95 nm diameter) is functionalized with 40 PEG molecules, each PEG molecule with molecular weight 5.04 kDa. We denote by $r_{max}(t)$ the instantaneous value for maximum distance between a PEG atom and CNT sidewall (Figure 5a) and denote by r(avg) the average over time of $r_{max}(t)$ value for every PEG molecule during a MD production run of 100 ps. The $r_{max}(t)$ value serves as a reference for the radial thickness of the polymer wrapping the carbon nanotube measured at every PEG molecule. We plot the r(avg) distribution along CNT (Figure 4b) and we consider the AFM instrument will be able to see only those PEG molecules with r(avg) higher than 60 Å. We therefore estimate the radial thickness (denoted as AFM) of the polymer wrapping CNT as the average of r(avg) values above AVG (60 Å) obtaining a AFM value of 76.2 Å which is very close to the 70 Å value reported from AFM measurements.[60]

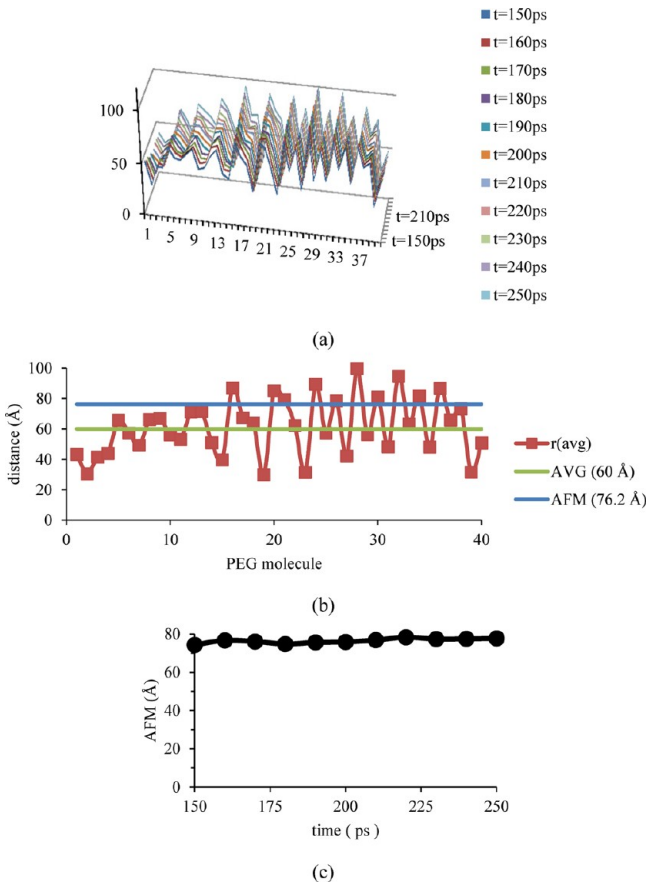

Figure 5. Estimation of polymer radial thicknes (AFM value) wrapping CNT. (a) Time evolution of $r_{max}(t)$, maximum distance between a PEG atom and CNT sidewall, for every PEG molecule. Vertical axis is in distance units (Å), horizontal axis is an identifier for PEG molecules with values 1, 2, ..., 40, and curves are color coded for different time (picoseconds); (b) AFM value estimation from r(avg) values. We calculate r(avg) for every PEG molecule as the average over time of $r_{max}(t)$ value in a 100 ps MD run. AVG is the average value of r(avg) and AFM is the average value of r(avg) when r(avg) is larger than AVG (60 Å); (c) AFM value estimation from instantaneous $r_{max}(t)$ values in a 100 ps MD run.

When we estimate the AFM value from the instantaneous $r_{max}(t)$ values, we obtain the time evolution of AFM value and observe an oscillation between 74.3 Å (minimum) and 78.3 Å (maximum) (Figure 5c). The very small oscillations, only ~2 Å deviation from average value for radial thickness of polymer wrapping CNT during the production run, justify the short time equilibration for the MD simulations.

The CNT of chirality (12,0) has a diameter ~1 nm which is the typical size reported on PEG–CNT complexes for drug delivery applications.[7,16,60,61] We define a twelve-atom CNT ring (Figure 6a) to which PEG molecules will be attached. To avoid overlap between PEGs attached to the same CNT ring; the linear segment of each PEG was elongated as much as possible, increasing PEG length in the radial direction (Figure 6b). To accommodate the maximum number of PEG molecules in a CNT ring, the linear segment of each PEG molecule is covalently linked to a carbon atom in the CNT ring (Figure 6c). To ensure maximum PEGylation, PEGs attached to different CNT rings were positioned as close as possible without overlap between PEGs (Figure 6d). This resulted in twelve PEG molecules attached to a CNT ring every 21.3 Å along the CNT

dx.doi.org/10.1021/jp305302y | J. Phys. Chem. B XXXX, XXX, XXX–XXX

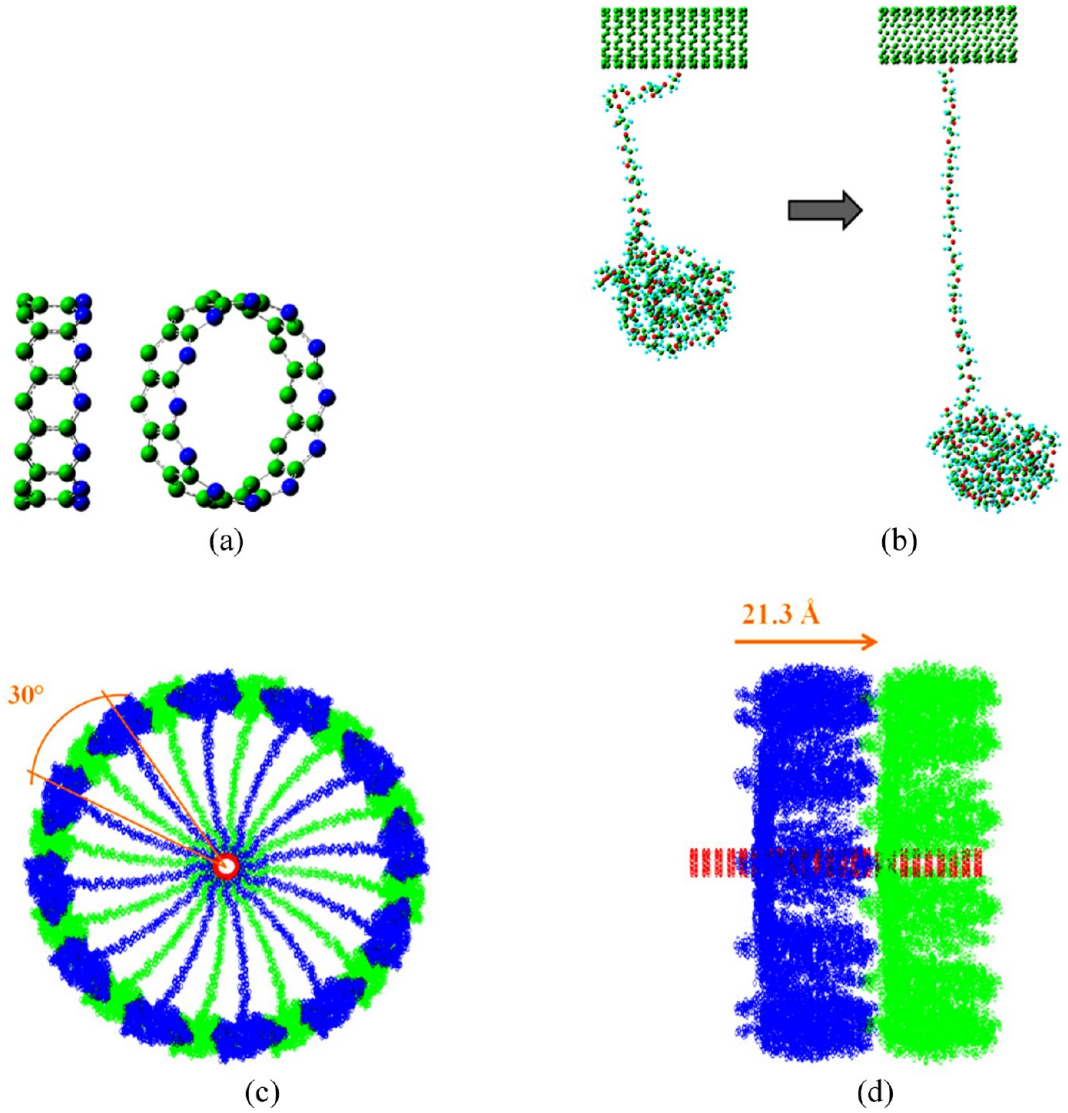

Figure 6. (a) Side views of a 12-atom carbon (blue) nanotube ring; there are four rings in this example (one blue and three greens). Some rings of the CNT will be chosen to be fully functionalized with PEG molecules. To achieve maximum PEGylation, (b) the linear segment of the PEG molecule is elongated, and (c,d) to avoid overlapping between PEG molecules attached to adjacent functionalized CNT rings, PEG molecules are shifted 15° between adjacent functionalized rings (green and blue). Twelve PEG molecules are attached to every CNT ring, and the distance between functionalized CNT rings is 21.3 Å.

sidewall. In total, 204 PEG molecules were attached to a 36.5 nm long single-walled CNT.

Molecular dynamics simulations were performed for the PEGylated CNT in a 380 × 190 × 190 Å^3 simulation box, 152 430 water molecules were added to solvate the construct. The initial O−C_1−C_2 angle at the CNT−PEG link was considered almost orthogonal (95°) and the initial angles C_0−C_1−C_2 in carbon nanotube were 120°. After an energy equilibration at room temperature (Figure 7a,b), the O−C_1−C_2 angle as well as the angles C_0−C_1−C_2 in carbon nanotube were gradually changed every 2 ps toward 104.5° (tetrahedral configuration, Figure 7c) in a 16 ps run (Figure 7d).

The MD simulation considered PEG molecules attached to the CNT sidewall and oriented orthogonal to the CNT axis. The possibility of PEGs linked to the CNT ends is then considered by adding two PEG molecules at each CNT end to the final PEG−CNT structure at 300 K (Figure 7e); in the new construct these PEG molecules have their linear segment oriented parallel to the CNT axis (Figure 8). The new PEG−CNT construct is placed in a 480 × 180 × 180 Å^3 simulation box solvated with 171 309 water molecules.

Room temperature was reached in a 50 ps linear ramp (Figure 9a), and 100 ps of energy equilibration at room temperature was required to observe a constant total potential energy (Figure 9b). The final structure for the equivalent model of a PEG−CNT is shown in Figure 9c.

The final structure from MD simulations with a single PEG molecule (Figure 3) is used to derive the CNT functionalized with 40 PEG molecules, the final structure from MD simulations with 40 PEGs (Figure 4) is used to derive the initial structure of CNT functionalized with 204 PEG molecules, and the final structure from MD simulations with 204 PEGs (Figure 7) is used to derive the initial structure of CNT functionalized with 208 PEG molecules, which final version is used for analysis and to draw conclusions.

We check that all PEG molecules stay covalently attached to the CNT during the MD runs. Shown below is a plot of CO bond length (Å) at every PEG−CNT link (n) from a MD run of 100 ps

dx.doi.org/10.1021/jp305302y | J. Phys. Chem. B XXXX, XXX, XXX−XXX

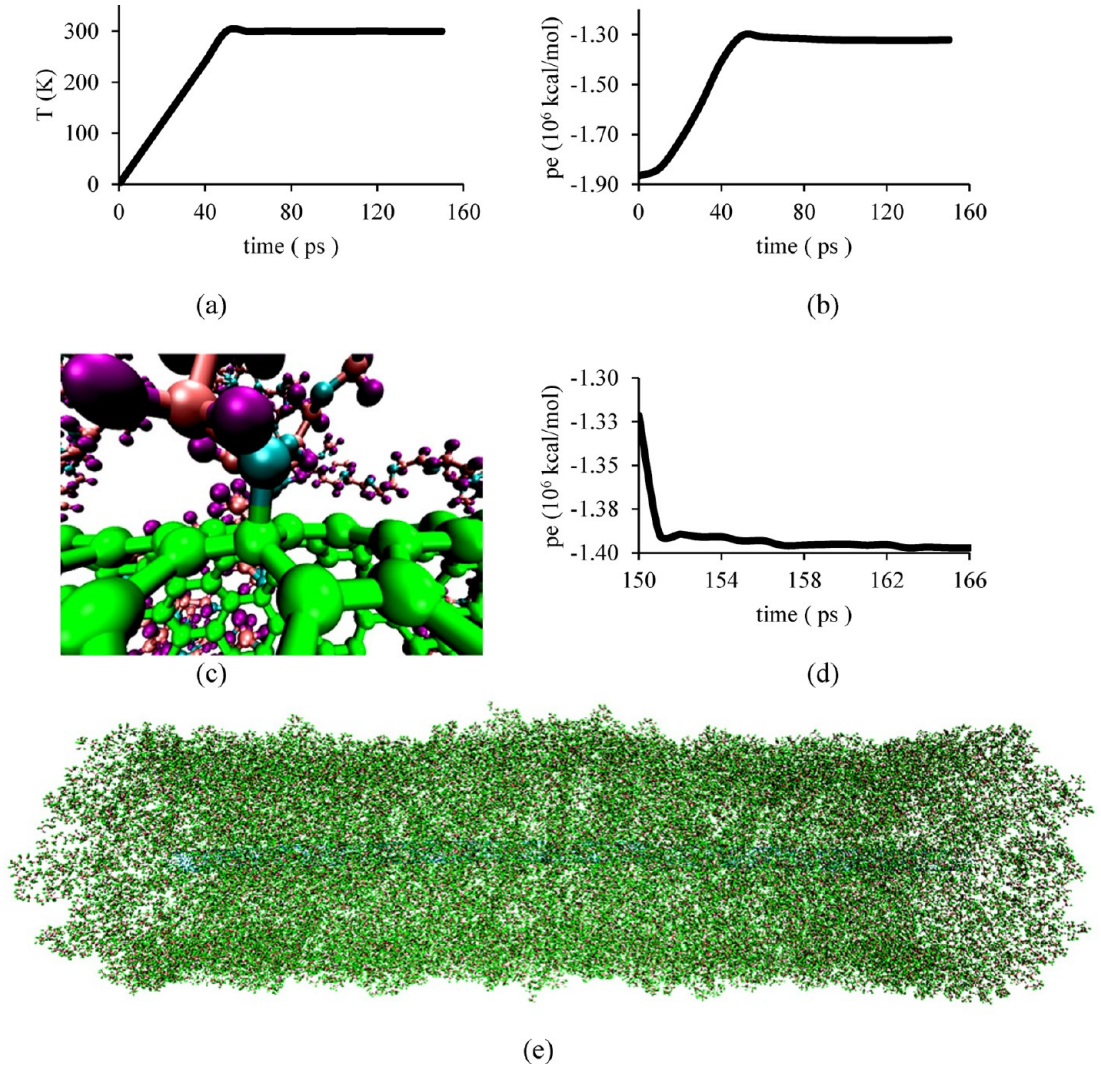

Figure 7. Time evolution of (a) temperature and (b) total potential energy for PEG−CNT construct with 204 PEG molecules. (c) Snapshot of final structure at 300K showing tetrahedral configuration at the PEG−CNT interface. Atoms are color coded: oxygen (cyan), carbon (orange), hydrogen (purple), and carbon nanotube (green). (d) Time evolution of total potential energy during gradual change of geometry at PEG−CNT interface from near orthogonal (OCC angle 95°) to tetrahedral (OCC angle 104.5°). (e) PEG−CNT at 300 K. Water molecules are omitted for visualization purposes.

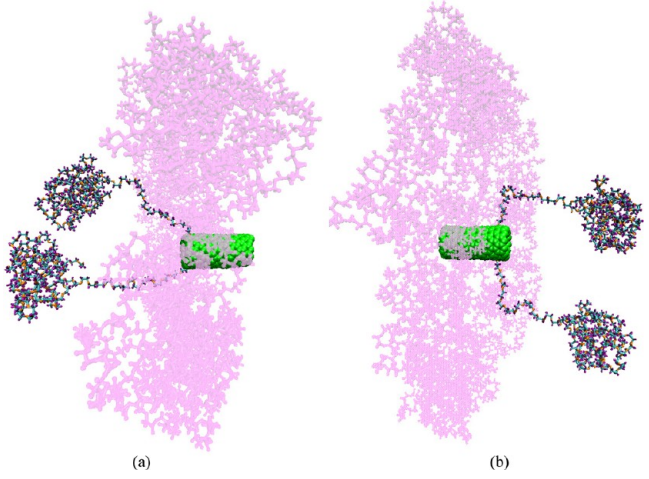

Figure 8. Building of initial structure. Schematic of four PEG molecules added to CNT ends, (a) two on the left side and (b) two on the right side. For visualization purposes only, a segment of CNT (green colored) is shown and other PEG molecules appear in purple color.

for the CNT functionalized with 40 (Figure 10a) and 208 PEG molecules (Figure 10b). Just by looking at the range of distances between a C from the CNT and the O from the PEG, we can make sure that all PEGs are chemically bonded to the CNT.

We calculate the interaction energies, including contributions from Coulombic and van der Waals forces as well as from bonded interactions. Bonded interactions include energy contributions coming from bonds, angles, and dihedrals in which the carbon and oxygen atoms from the PEG and CNT are covalently bonded. The interaction energy per PEGmer is −9.2 and −10.3 kcal/mol for the PEG40-CNT and PEG208-CNT, respectively. These relatively close energy values (Table 7) provide evidence that full PEGylation is feasible in the CNT−PEG systems.

If $\hat{k}$ is a unitary vector in the CNT axial direction and $\overline{w_p}$ the vector between a PEG atom and the CNT atom to which the PEG molecule is covalently linked, we can calculate r_{uvp}, the distance between a PEG atom and the CNT sidewall, as

$$r_{uvp} = \text{norm}(\overline{w_p} - (\overline{w_p}\cdot\hat{k})\hat{k}) \quad (4)$$

dx.doi.org/10.1021/jp305302y | J. Phys. Chem. B XXXX, XXX, XXX−XXX

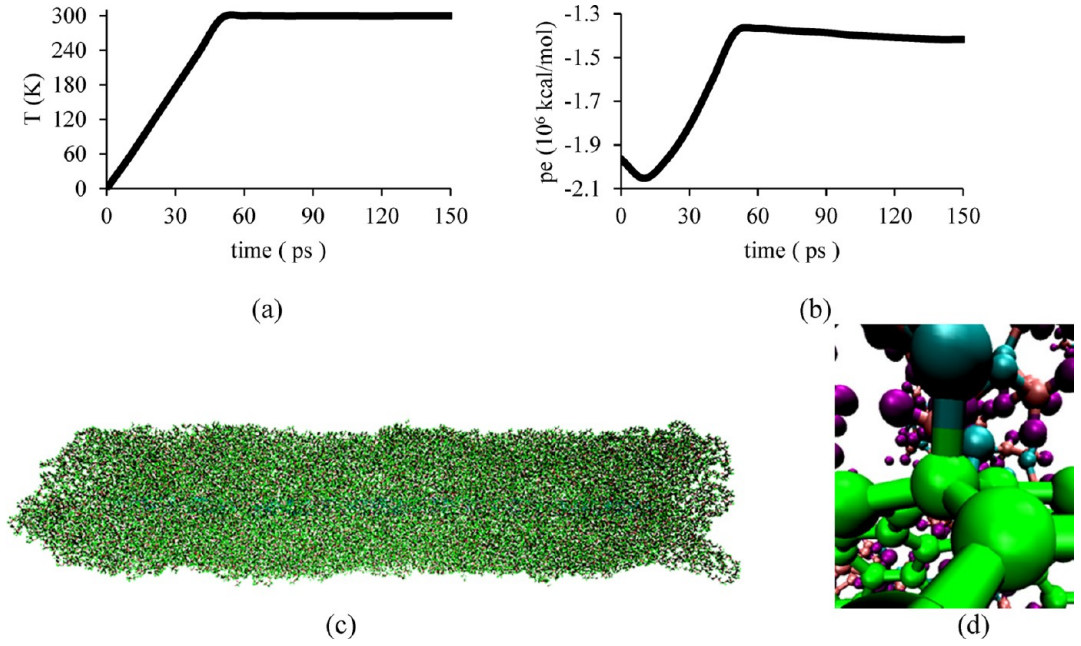

Figure 9. Time evolution of (a) temperature and (b) total potential energy for PEG−CNT construct with 208 PEG molecules. (c) PEG−CNT structure at t = 150 ps and room temperature, and (d) tetrahedral structure at a PEG−CNT link.

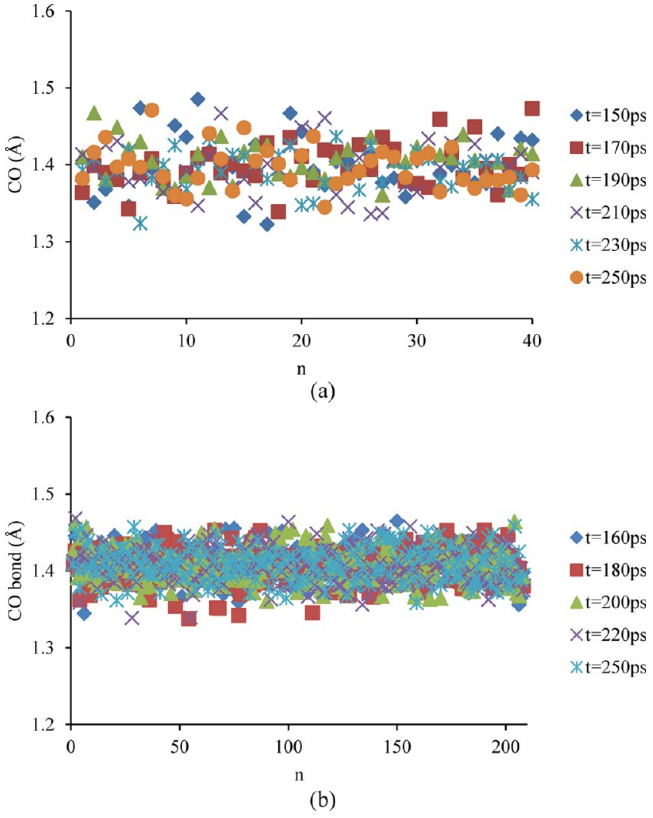

Figure 10. Carbon−oxygen bond distance at every PEG−CNT link for the CNT functionalized with (a) 40 PEG molecules and (b) 208 PEG molecules. n is the bookkeeping index for the PEG−CNT links in the complex.

Therefore, the maximum distance between a PEG atom and CNT sidewall is defined as (Figure 11)

$$r_{uv} = \max(|r_{uv(1)}|, ..., |r_{uv(799)}|) \quad (5)$$

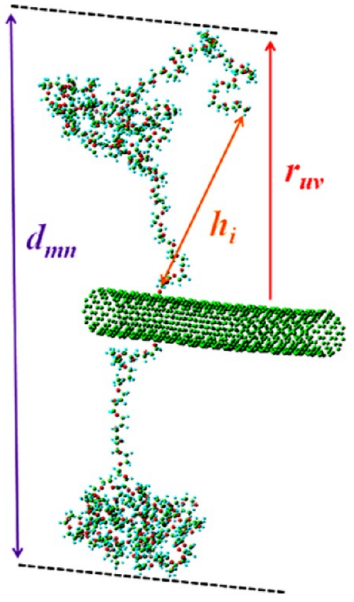

Figure 11. Distances calculated in the PEG−CNT complex. d_{mn} is the maximum distance between atoms of opposite PEG molecules attached to a same CNT ring and along a direction orthogonal to the CNT axis, m is an index for every CNT ring, and n is an index for every pair of opposite PEG molecules attached to the ring. h_i is the end-to-end distance for every PEG molecule. r_{uv} is the maximum distance between a PEG atom and the CNT sidewall, u is an index for every CNT ring, and v is an index for every PEG molecule attached to the ring.

Twelve PEG molecules are attached to every CNT ring (Figure 6c); therefore, we define

$$r_u = \max(|r_{u(1)}|, ..., |r_{u(12)}|) \quad (6)$$

Calculus of d_{mn} is to estimate the width of our PEG−CNT construct at every section corresponding to a CNT ring, so on the basis of the geometry of opposite PEG molecules n_1 and n_2 (Figure 11), we define

dx.doi.org/10.1021/jp305302y | J. Phys. Chem. B XXXX, XXX, XXX−XXX

Table 7. Interaction Energy of the PEG−CNT Complex, Averaged over the Last 50 ps of the MD Simulation[a]

energy (kcal/mol)	PEG40-CNT	PEG208-CNT
total	-4.176×10^4	-2.443×10^5
per PEG molecule	-1.044×10^3	$-1.175\text{E} \times 10^3$
per PEGmer	−9.16	−10.30

[a]Each PEG molecule is a 114-mer. Interaction energy includes contributions from noncovalent interactions over the whole complex and contributions from bonded interactions at the PEG−CNT link.

$$d_{mn} = r_{mn_1} + r_{mn_2} + \text{CNT}_{\text{diameter}} \quad (7)$$

and

$$d_m = \max(|d_{m(1)}|, \ldots, |d_{m(6)}|) \quad (8)$$

The PEG−CNT construct has 17 rings with attachment of 12 PEG molecules; r_u and d_m have different values at each of those CNT rings. If h_i is the end-to-end distance for every PEG molecule, we define h_i^{rms} as the corresponding root-mean-squared end-to-end distance. After the equilibration at 300 K, we estimate the minimum, average, and maximum values for r_u and h_i^{rms} for the PEG−CNT complex with 40 PEGs (Figure 12), and we estimate the minimum, average, and maximum values for r_u, d_m, and h_i^{rms} for the PEG−CNT complex with 208 PEGs (Figure 13). We calculate also the maximum length (L_{max}) of the PEG−CNT construct with 208 PEGs (Figure 9c) as the maximum distance between atoms of PEG molecules attached to CNT ends. Therefore, we are using the final runs of the 40 and 208 PEG molecules (Figures 12 and 13) to draw our conclusions. We observe small oscillations of only ∼2 Å in the average values for the radial thickness of polymer wrapping CNT, and thus, we have enough statistics to draw conclusions.

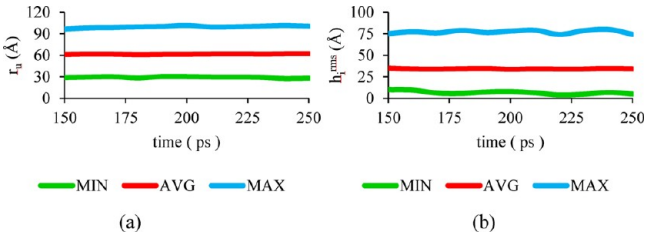

Figure 12. Estimates for a PEG−CNT construct with 40 PEG molecules. (a) Maximum distance between a PEG atom and CNT sidewall, and (b) root-mean-squared end-to-end distance for a PEG molecule.

For a PEG−CNT complex with 40 PEG molecules, we observe for the maximum r_u a large value of 100.3 Å (Figure 12a) which indicates some PEG molecules elongates adopting a linear conformation and it would imply poor trapping of drug molecules. In our MD simulations of PEG−CNT in water solvent, one end of each PEG molecule is linked to the CNT sidewall. For the minimum h_i^{rms} we observe a small value of 5.3 Å (Figure 12b); this is due to some (hydrophilic) PEG molecules having enough freedom or space to wrap around the hydrophobic carbon nanotube and imply a not efficient covering of hydrophobic sites since we prefer the highest surface of hydrophobic carbon nanotube free of PEG wrapping to ensure sequestration of a hydrophobic drug. Furthermore, we observe a root-mean-squared end-to-end distance value of 34.2 Å (Figure 12b) for a PEG molecule linked to the CNT and this value is very close to the value of 35 Å (Figure 3c) observed for a single PEG molecule in water solvent.

The maximum and minimum values for r_u and h_i^{rms} are closer to the average value in the complex with 208 PEG molecules (Figure 13a,b) than in the complex with 40 PEGs (Figure 12a,b),

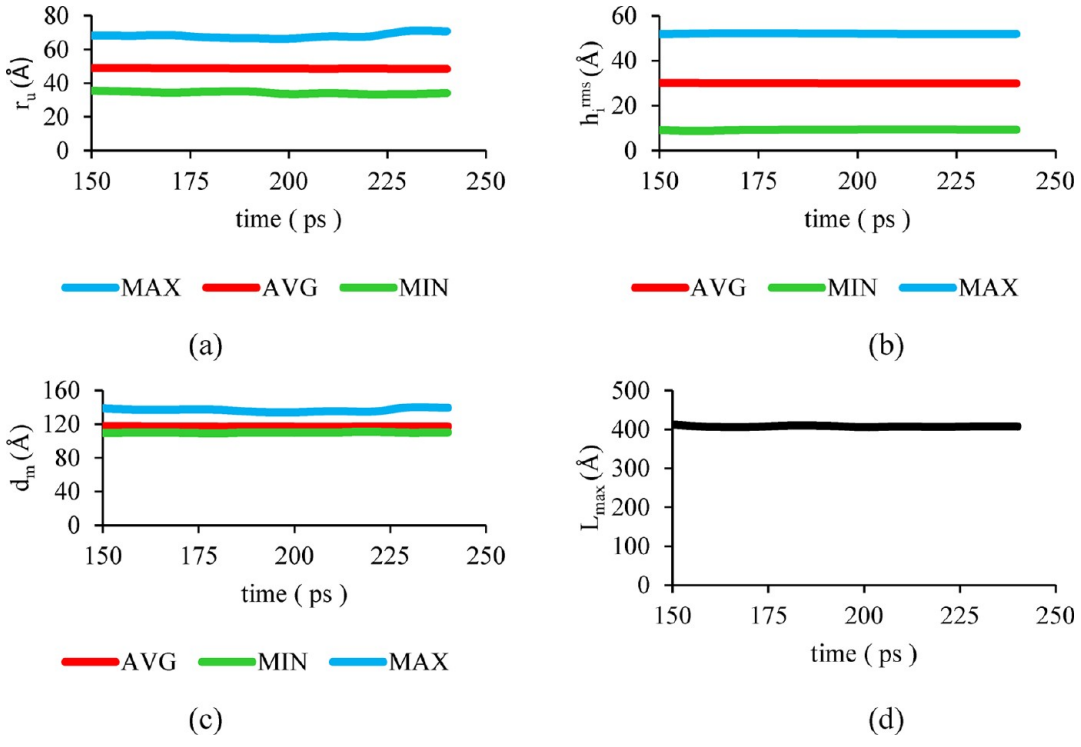

Figure 13. Estimates for a PEG−CNT complex including 208 PEG molecules. (a) Maximum distance between a PEG atom and CNT sidewall, (b) root-mean-squared end-to-end distance, (c) width of the PEG−CNT complex has a maximum value of 136.5 Å (averaged during the last 50 ps), and (d) the maximum length of the PEG−CNT complex is 407 Å (averaged during the last 50 ps).

dx.doi.org/10.1021/jp305302y | J. Phys. Chem. B XXXX, XXX, XXX−XXX

meaning we have a more homogeneous size distribution of PEG molecules, with no PEG molecule wrapping the carbon nanotube surface and no PEG molecule in linear (elongated) conformation. Furthermore, we noticed a root-mean-squared end-to-end distance value of 29.9 Å, averaged on 208 PEG molecules (AVG value in Figure 13b). This distance is smaller than the value of 35 Å (Figure 3c) observed for a single PEG molecule in water solvent and smaller than the value 34.2 Å observed in a complex with 40 PEGs (Figure 12b). It is noticeable that this occurred when maximum PEGylation was induced by having only 21.3 Å spacing between PEG molecules along the CNT axis direction (Figure 6d). We attribute this to the induced maximum PEGylation and to a hydrophobic effect: the PEG molecules adopt a structural conformation which prevents water molecules from reaching the hydrophobic carbon nanotube sidewall; maximum PEGylation ensures an efficient protection of hydrophobic sites. In the case of HCCs, we suggest that this ensures better sequestration of drug molecules, since PEG molecules would allow hydrophobic drug molecules to reach a hydrophobic site in the HCC. We also suggest that drug liberation occurs mainly during PEG−HCC translocation through the cell membrane or inside the crowded cytoplasm; during these processes, stronger or more frequent interactions with biological molecules would affect or dominate PEG molecular conformation.

For the PEG−CNT construct with 208 PEG molecules, the resultant average values for r_u and d_m are 48.5 Å (Figure 13a) and 136.5 Å (Figure 13b), which are indicative of PEG size contribution to the PEG−HCC construct. We also noticed that the r_u maximum (68.7 Å) and r_u average (48.5 Å) are smaller than the values of 100.3 and 61.9 Å (Figures 12a and 13a) observed in a construct with only 40 PEGs. These suggest that a more homogeneous and smaller size distribution for PEG molecules is attained when approaching maximum PEGylation. Thus, a 114-mer PEG is short enough to obtain a width size within the nano regime, adequate for drug delivery platforms.

From our MD simulations at temperatures above 300 K, we observe a tendency for PEG molecules to elongate toward linear conformations in which case it should be feasible attaching a higher number of PEG molecules to CNT sidewall. We suggest therefore performing PEGylation at high temperatures but further research is required to estimate the optimal temperature and conditions to achieve maximum PEGylation.

SUMMARY AND CONCLUSIONS

We performed molecular dynamics calculations on the real size of a PEG−CNT in a bath of water. The PEG was 114 units long and terminated with oxygen atoms at both ends. It was placed at the center of a cubic box 80 Å long with 16 500 water molecules, and the temperature was increased from 0.1 to 300 K in a 50 ps linear ramp followed by equilibration at 300 K for 1.05 ns until the root-mean-squared end-to-end distance of the PEG was almost constant. During this equilibration, the PEG molecule adopted a globular shape. From this equilibration, the last structural configuration for PEG was taken as a reference and used to construct a PEGylated CNT. The MD simulation considered PEG molecules attached to the CNT sidewall and oriented orthogonal to the CNT axis. The possibility of PEGs linked to the CNT ends was considered by adding two PEG molecules at each end of the final PEG−CNT at 300 K; these four PEG molecules were oriented parallel to the CNT axis. The PEG−CNT was placed in a 480 × 180 × 180 $Å^3$ simulation box with 171 309 water molecules. After averaging for 50 ps of production runs, the width of the PEG−CNT complex reaches a maximum value of 136.5 Å and the maximum length of the full PEG−CNT complex is 407 Å. Through this modeling of a shortened single-walled carbon nanotube as the central core with 5040 molecular weight PEG addends, an approximation of the hydrodynamic volume of a PEG−CNT (and by extension, a PEG−HCC) is attained. Indeed, even in their hydrated form, as shown here, the PEG−CNT remains well within the nanosized (40 nm) regime, providing a rational for their observed rapid clearance through the kidneys of mammals.[7] We elucidate the advantage of the hydrophilic character of PEG molecules and of maximum PEGylation, both favoring an optimal capture, protection, and controlled release of drug molecules.

Approaching maximum PEGylation yields a decrease in radial thickness of polymer covering the CNT and a decrease in the probability for PEG wrapping of the CNT, and prevents water molecules from reaching the CNT. In the case of HCCs, maximum PEGylation ensures better sequestration of drug molecules, since a decrease in the probability for PEG wrapping the CNT implies a higher surface area of hydrophobic sites available to capture drug molecules and a decrease in polymer radial thickness produces a denser polymer and therefore better protection of drug molecules from water.

Maximum PEGylation should be therefore considered an important design constraint to achieve an optimal drug delivery platform providing the ability of efficient release of drug molecules.

AUTHOR INFORMATION

Corresponding Author

*Tel.: (979)845-3301 (J.M.S.); 713-348-6246 (J.M.T.). Fax: (979)845-3301 (J.M.S.); 713-348-6250 (J.M.T.). E-mail: seminario@tamu.edu (J.M.S.); tour@rice.edu (J.M.T.).

Notes

The authors declare no competing financial interest.

ACKNOWLEDGMENTS

The research at Texas A&M was supported by the U.S. Defense Threat Reduction Agency (DTRA) through the U.S. Army Research Office (ARO) under grant no. W911NF-06-1-0231, and the ARO under a MURI Project # W911NF-11-1-0024 and we also acknowledge the Texas A&M Supercomputing Center. The research at Rice University was supported by the Department of Defense Traumatic Brain Injury-Houston Medical Center consortium through the USAMRAA (W81XWH-08-2-0143).

REFERENCES

(1) Bottini, M.; Rosato, N.; Bottini, N. PEG-Modified Carbon Nanotubes in Biomedicine: Current Status and Challenges Ahead. *Biomacromolecules* **2011**, *12*, 3381−3393.

(2) Heister, E.; Neves, V.; Lamprecht, C.; Silva, S. R. P.; Coley, H. M.; McFadden, J. Drug loading, dispersion stability, and therapeutic efficacy in targeted drug delivery with carbon nanotubes. *Carbon* **2012**, *50*, 622−632.

(3) Jin, H.; Heller, D. A.; Sharma, R.; Strano, M. S. Size-Dependent Cellular Uptake and Expulsion of Single-Walled Carbon Nanotubes: Single Particle Tracking and a Generic Uptake Model for Nanoparticles. *ACS Nano* **2009**, *3*, 149−158.

(4) Chen, Z.; Kobashi, K.; Rauwald, U.; Booker, R.; Fan, H.; Hwang, W.-F.; Tour, J. M. Soluble Ultra-Short Single-Walled Carbon Nanotubes. *J. Am. Chem. Soc.* **2006**, *128*, 10568−10571.

(5) Price, B. K.; Lomeda, J. R.; Tour, J. M. Aggressively Oxidized Ultra-Short Single-Walled Carbon Nanotubes Having Oxidized Sidewalls. *Chem. Mater.* **2009**, *21*, 3917−3923.

(6) Stephenson, J. J.; Hudson, J. L.; Leonard, A. D.; Price, B. K.; Tour, J. M. Repetitive Functionalization of Water-Soluble Single-Walled Carbon

Nanotubes. Addition of Acid-Sensitive Addends. *Chem. Mater.* **2007**, *19*, 3491−3498.
(7) Berlin, J. M.; Leonard, A. D.; Pham, T. T.; Sano, D.; Marcano, D. C.; Yan, S.; Fiorentino, S.; Milas, Z. L.; Kosynkin, D. V.; Price, B. K.; Lucente-Schultz, R. M.; Wen, X.; Raso, M. G.; Craig, S. L.; Tran, H. T.; Myers, J. N.; Tour, J. M. Effective Drug Delivery, In Vitro and In Vivo, by Carbon-Based Nanovectors Noncovalently Loaded with Unmodified Paclitaxel. *ACS Nano* **2010**, *4*, 4621−4636.
(8) Sano, D.; Berlin, J. M.; Pham, T. T.; Marcano, D. C.; Valdecanas, D. R.; Zhou, G.; Milas, L.; Myers, J. N.; Tour, J. M. Noncovalent Assembly of Targeted Carbon Nanovectors Enables Synergistic Drug and Radiation Cancer Therapy in Vivo. *ACS Nano* **2012**, *6*, 2497−2505.
(9) Sharpe, M. A.; Marcano, D. C.; Berlin, J. M.; Widmayer, M. A.; Baskin, D. S.; Tour, J. M. Antibody-Targeted Nanovectors for the Treatment of Brain Cancers. *ACS Nano* **2012**, *6*, 3114−3120.
(10) Cheng, J.; Fernando, K. A. S.; Veca, L. M.; Sun, Y.-P.; Lamond, A. I.; Lam, Y. W.; Cheng, S. H. Reversible Accumulation of PEGylated Single-Walled Carbon Nanotubes in the Mammalian Nucleus. *ACS Nano* **2008**, *2*, 2085−2094.
(11) Zhang, P.; Henthorn, D. B. Synthesis of PEGylated single wall carbon nanotubes by a photoinitiated graft from polymerization. *AIChE J.* **2010**, *56*, 1610−1615.
(12) Nie, H.; Guo, W.; Yuan, Y.; Dou, Z.; Shi, Z.; Liu, Z.; Wang, H.; Liu, Y. PEGylation of double-walled carbon nanotubes for increasing their solubility in water. *Nano Res.* **2010**, *3*, 103−109.
(13) Di, L.; Kerns, E. H.; Li, S. Q.; Petusky, S. L. High throughput microsomal stability assay for insoluble compounds. *Int. J. Pharm.* **2006**, *317*, 54−60.
(14) Lipinski, C. A. Drug-like properties and the causes of poor solubility and poor permeability. *J. Pharmacol. Toxicol.* **2000**, *44*, 235−249.
(15) Hummer, G.; Rasaiah, J. C.; Noworyta, J. P. Water conduction through the hydrophobic channel of a carbon nanotube. *Nature* **2001**, *414*, 188−190.
(16) Chee Leng, L.; Hui Qi, L.; Hui Ru, T.; Ye, L. Delivery of paclitaxel by physically loading onto poly(ethylene glycol) (PEG)-graftcarbon nanotubes for potent cancer therapeutics. *Nanotechnology* **2010**, *21*, 065101.
(17) Cronin, M. T. D. The Role of Hydrophobicity in Toxicity Prediction. *Curr. Comput.-Aid. Drug* **2006**, *2*, 405−413.
(18) Moyano, D. F.; Goldsmith, M.; Solfiell, D. J.; Landesman-Milo, D.; Miranda, O. R.; Peer, D.; Rotello, V. M. Nanoparticle Hydrophobicity Dictates Immune Response. *J. Am. Chem. Soc.* **2012**, *134*, 3965−3967.
(19) Veronese, F. M.; Pasut, G. PEGylation, successful approach to drug delivery. *Drug Discov. Today* **2005**, *10*, 1451−1458.
(20) Bobadilla, A. D.; Seminario, J. M. DNA−CNT Interactions and Gating Mechanism Using MD and DFT. *J. Phys. Chem. C* **2011**, *115*, 3466−3474.
(21) Bellido, E. P.; Seminario, J. M. Molecular Dynamics Simulations of Folding of Supported Graphene. *J. Phys. Chem. C* **2010**, *114*, 22472−22477.
(22) Rangel, N. L.; Sotelo, J. C.; Seminario, J. M. Mechanism of carbon nanotubes unzipping into graphene ribbons. *J. Chem. Phys.* **2009**, *131*, 031105−4.
(23) Borhani, D.; Shaw, D. The future of molecular dynamics simulations in drug discovery. *J. Comput.-Aided Mol. Des.* **2012**, *26*, 15−26.
(24) Li, Y.; Hou, T. Computational Simulation of Drug Delivery at Molecular Level. *Curr. Med. Chem.* **2010**, *17*, 4482−4491.
(25) Salazar, P. F.; Seminario, J. M. Identifying Receptor−Ligand Interactions through an ab Initio Approach. *J. Phys. Chem. B* **2008**, *112*, 1290−1292.
(26) Johnson, B. C.; Metifiot, M.; Pommier, Y.; Hughes, S. H. Molecular Dynamics Approaches Estimate the Binding Energy of HIV-1 Integrase Inhibitors and Correlate with In Vitro Activity. *Antimicrob. Agents Chemother.* **2012**, *56*, 411−419.
(27) Åqvist, J.; Luzhkov, V. B.; Brandsdal, B. O. Ligand Binding Affinities from MD Simulations. *Acc. Chem. Res.* **2002**, *35*, 358−365.
(28) Durrant, J. D.; McCammon, J. A. Molecular dynamics simulations and drug discovery. *BMC Biol.* **2011**, 9.
(29) MacKerell, A. D.; Bashford, D.; Bellott, R. L.; Dunbrack, J. D.; Evanseck, M. J.; Field, S.; Fischer, J.; Gao, H.; Guo, S.; Ha, D.; Joseph-McCarthy, L.; Kuchnir, K.; Kuczera, F. T. K.; Lau, C.; Mattos, S.; Michnick, T.; Ngo, D. T.; Nguyen, B.; Prodhom, W. E.; Reiher, B.; Roux, M.; Schlenkrich, J. C.; Smith, R.; Stote, J.; Straub, M.; Watanabe, J.; Wiórkiewicz-Kuczera, D.; Yin; Karplus, M. All-Atom Empirical Potential for Molecular Modeling and Dynamics Studies of Proteins. *J. Phys. Chem. B* **1998**, *102*, 3586−3616.
(30) Foloppe, N.; MacKerell, J. A. D. All-atom empirical force field for nucleic acids: I. Parameter optimization based on small molecule and condensed phase macromolecular target data. *J. Comput. Chem.* **2000**, *21*, 86−104.
(31) Feller, S. E.; MacKerell, A. D. An Improved Empirical Potential Energy Function for Molecular Simulations of Phospholipids. *J. Phys. Chem. B* **2000**, *104*, 7510−7515.
(32) Vorobyov, I.; Anisimov, V. M.; Greene, S.; Venable, R. M.; Moser, A.; Pastor, R. W.; MacKerell, A. D. Additive and Classical Drude Polarizable Force Fields for Linear and Cyclic Ethers. *J. Chem. Theory Comput.* **2007**, *3*, 1120−1133.
(33) Mayo, M. L.; Chen, Z. Q.; Kilina, S. V. Computational Studies of Nucleotide Selectivity in DNA−Carbon Nanotube Hybrids. *J. Phys. Chem. Lett.* **2012**, *3*, 2790−2797.
(34) Furmanchuk, A. o.; Leszczynski, J.; Tretiak, S.; Kilina, S. V. Morphology and Optical Response of Carbon Nanotubes Functionalized by Conjugated Polymers. *J. Phys. Chem. C* **2012**, *116*, 6831−6840.
(35) Yarotski, D. A.; Kilina, S. V.; Talin, A. A.; Tretiak, S.; Prezhdo, O. V.; Balatsky, A. V.; Taylor, A. J. Scanning Tunneling Microscopy of DNA-Wrapped Carbon Nanotubes. *Nano Lett.* **2008**, *9*, 12−17.
(36) Vanommeslaeghe, K.; Hatcher, E.; Acharya, C.; Kundu, S.; Zhong, S.; Shim, J.; Darian, E.; Guvench, O.; Lopes, P.; Vorobyov, I.; Mackerell, A. D. CHARMM general force field: A force field for drug-like molecules compatible with the CHARMM all-atom additive biological force fields. *J. Comput. Chem.* **2010**, *31*, 671−690.
(37) Lee, H.; Venable, R. M.; MacKerell, A. D.; Pastor, R. W. Molecular Dynamics Studies of Polyethylene Oxide and Polyethylene Glycol: Hydrodynamic Radius and Shape Anisotropy. *Biophys. J.* **2008**, *95*, 1590−1599.
(38) Plimpton, S. Fast parallel algorithms for short-range molecular dynamics. *J. Comput. Phys.* **1995**, *117*, 1−19.
(39) Tasaki, K. Poly(oxyethylene)−cation interactions in aqueous solution: a molecular dynamics study. *Comput. Theor. Polym. Sci.* **1999**, *9*, 271−284.
(40) Huang, B.-D.; Xia, Y.-Y.; Zhao, M.-W.; Li, F.; Liu, X.-D.; Ji, Y.-J.; Song, C.; Tan, Z.-Y.; Liu, H. Single-Walled Carbon Nanotubes Acting as Controllable Transport Channels. *Chin. Phys. Lett.* **2004**, *21*, 2388.
(41) Noon, W. H.; Ausman, K. D.; Smalley, R. E.; Ma, J. Helical ice-sheets inside carbon nanotubes in the physiological condition. *Chem. Phys. Lett.* **2002**, *355*, 445−448.
(42) Guo, C. Y.; Montgomery Pettitt, B.; Wheeler, L. T. Force field comparisons of the heat capacity of carbon nanotubes. *Mol. Simul.* **2006**, *32*, 839−848.
(43) Jorgensen, W. L.; Chandrasekhar, J.; Madura, J. D.; Impey, R. W.; Klein, M. L. Comparison of simple potential functions for simulating liquid water. *J. Chem. Phys.* **1983**, *79*, 926−935.
(44) Politzer, P.; Seminario, J.; Bolduc, P. A Proposed Interpretation of the Destabilizing Effect of Hydroxyl-Groups on Nitroaromatic Molecules. *Chem. Phys. Lett.* **1989**, *158*, 463−469.
(45) Murray, J.; Redfern, P.; Seminario, J.; Politzer, P. Anomalous Energy Effects in some Aliphatic and Alicyclic Aza Systems and their Nitro-Derivatives. *J. Phys. Chem.* **1990**, *94*, 2320−2323.
(46) Murray, J. S.; Seminario, J. M.; Politzer, P. Does Antiaromaticity Imply Net Destabilization. *Int. J. Quantum Chem.* **1994**, *49*, 575−579.
(47) Seminario, J. M.; Concha, M. C.; Politzer, P. Calculated structures and relative stabilities of furoxan, some 1,2-dinitrosoethylenes and other isomers. *J. Comput. Chem.* **1992**, *13*, 177−182.
(48) Choi, D.-S.; Huang, S.; Huang, M.; Barnard, T. S.; Adams, R. D.; Seminario, J. M.; Tour, J. M. Revised Structures of N-Substituted

Dibrominated Pyrrole Derivatives and Their Polymeric Products. Termaleimide Models with Low Optical Band Gaps. *J. Org. Chem.* **1998**, 63−2655.
(49) Seminario, J. M.; Concha, M. C.; Politzer, P. A Density Functional/Molecular Dynamics of the Structure of Liquid Nitromethane. *J. Chem. Phys.* **1995**, *102*, 8281−8282.
(50) Seminario, J. M.; Concha, M. C.; Murray, J. S.; Politzer, P. Theoretical Analyses of O_2/H_2O Systems under Normal and Supercritical Conditions. *Chem. Phys. Lett.* **1994**, *222*, 25−32.
(51) Seminario, J. M.; Derosa, P. A.; Cordova, L. E.; Bozard, B. H. A molecular device operating at terahertz frequencies: theoretical simulations. *IEEE Trans. Nanotechnol.* **2004**, *3*, 215−218.
(52) Polak, E.; Ribiere, G. Note sur la convergence de méthodes de directions conjuguées. *Rev. Fr. Inform. Rech. Oper.* **1969**, *3*, 35−43.
(53) Andersen, H. C. Molecular dynamics simulations at constant pressure and/or temperature. *J. Chem. Phys.* **1980**, *72*, 2384−2393.
(54) Hoover, W. G. Canonical dynamics: Equilibrium phase-space distributions. *Phys. Rev. A* **1985**, *31*, 1695−1697.
(55) Shinoda, W.; Shiga, M.; Mikami, M. Rapid estimation of elastic constants by molecular dynamics simulation under constant stress. *Phys. Rev. B* **2004**, *69*, 134103.
(56) Humphrey, W. VMD: Visual molecular dynamics. *J. Mol. Graphics* **1996**, *14*, 33−38.
(57) Martínez, L.; Andrade, R.; Birgin, E. G.; Martínez, J. M. PACKMOL: A package for building initial configurations for molecular dynamics simulations. *J. Comput. Chem.* **2009**, *30*, 2157−2164.
(58) French, A. C.; Thompson, A. L.; Davis, B. G. High-Purity Discrete PEG-Oligomer Crystals Allow Structural Insight. *Angew. Chem. Int. Ed.* **2009**, *48*, 1248−1252.
(59) Lee, H.; de Vries, A. H.; Marrink, S.-J.; Pastor, R. W. A Coarse-Grained Model for Polyethylene Oxide and Polyethylene Glycol: Conformation and Hydrodynamics. *J. Phys. Chem. B* **2009**, *113*, 13186−13194.
(60) Hong, G.; Wu, J. Z.; Robinson, J. T.; Wang, H.; Zhang, B.; Dai, H. Three-dimensional imaging of single nanotube molecule endocytosis on plasmonic substrates. *Nat. Commun.* **2012**, *3*, 700.
(61) Bhirde, A. A.; Patel, S.; Sousa, A. A.; Patel, V.; Molinolo, A. A.; Ji, Y.; Leapman, R. D.; Gutkind, J. S.; Rusling, J. F. Distribution and clearance of PEG-single-walled carbon nanotube cancer drug delivery vehicles in mice. *Nanomedicine* **2010**, *5*, 1535−1546.